Int. J. Heat Mass Transfer. Vol. 25, No. 1, pp. 137–147, 1982.
Printed in Great Britain

0017-9310/82/010137-11 $03.00/0
Pergamon Press Ltd.

ANALYSIS OF THE HEAT TRANSPORT MECHANISMS DURING MELTING AROUND A HORIZONTAL CIRCULAR CYLINDER*

H. RIEGER, U. PROJAHN and H. BEER
Institut für Technische Thermodynamik, Technische Hochschule Darmstadt, Petersenstrasse 30, 6100 Darmstadt, Federal Republic of Germany

(*Received* 22 *May* 1981)

Abstract—The melting process around a heated horizontal circular cylinder embedded in a phase change material has been analyzed by means of numerical methods. Both heat conduction and convection have been taken into account to treat this moving boundary problem. Difficulties associated with the complex structure of the timewise changing physical domain (melt region) have been successfully overcome by applying a numerical mapping technique (body-fitted coordinates).

Numerical solutions have been obtained for Rayleigh numbers up to $Ra = 1.5 \cdot 10^5$, Stefan numbers in the range $0.005 \leqq Ste \leqq 0.08$ and for $Pr = 50$. The results are discussed in detail and indicate that the influence of natural convection has to be considered in all cases.

NOMENCLATURE

a, thermal diffusivity;
$A, \bar{A}$, finite difference operators (equation 26);
c_p, specific heat;
$\mathbf{e}_1, \mathbf{e}_2$, normal unit vectors in x, y direction;
f, F, dummy variables;
Fo, $= a \cdot \tau / R_0^2$, Fourier number;
g, acceleration due to gravity;
$\mathbf{G}$ $= (0, -g, 0)$, gravitation vector;
h, film heat-transfer coefficient;
h_f, latent heat of fusion;
i, j, integer variables;
J, $= x_\xi y_\eta - x_\eta y_\xi$, Jacobian of transformation;
$L^f F$, $= [(f_\eta F)_\xi - (f_\xi F)_\eta]/J$, operator;
n, coordinate in normal direction;
Nu, $= h \cdot R_0/\lambda$, Nusselt number;
P, Q, coordinate control functions;
Pr, $= \nu/a$, Prandtl number;
Ra, $= g\bar{\beta} R_0^3 (T_w - T_f)/(\nu a)$, Rayleigh number;
r, distance from center of cylinder to solid–liquid interface;
R_c, characteristic radius (equation 37);
R_0, radius of cylinder;
S, shifting operator (equation 33);
Ste, $= c_p (T_w - T_f)/h_f$, Stefan number;
t, time;
T, temperature;
u, v, velocity components along x, y direction;
V, $\int_0^\pi \int_{R_0}^r r(\varphi) \mathrm{d}r \, \mathrm{d}\varphi$, volume of melt region;
$\mathbf{w}$, $= (u, v, 0)$, velocity vector;
x, y, Cartesian coordinate directions in physical plane.

Greek symbols

α, β, γ, transformation factors ($\alpha = x_\eta^2 + y_\eta^2$; $\beta = x_\xi x_\eta + y_\xi y_\eta$; $\gamma = x_\xi^2 + y_\xi^2$);
$\bar{\beta}$, thermal expansion coefficient;
$\delta, \bar{\delta}$, finite difference operators (equation 26);
θ, $= (T - T_f)/(T_w - T_f)$, dimensionless temperature;
λ, thermal conductivity;
ν, kinematic viscosity;
ξ, η, coordinate directions in transformed plane;
ρ, density;
τ, $= Fo \cdot Ste$, dimensionless time;
ϕ, χ, parameters of control functions;
φ, angle;
ψ, stream function;
$\mathbf{\Psi}$, $= (0, 0, \psi)$, vector potential;
ω, $= v_x - u_y$, vorticity;
$\mathbf{\Omega}$ $= (0, 0, \omega)$, vorticity vector;
∇, $= \mathbf{e}_1 \partial_x + \mathbf{e}_2 \partial_y$, nabla operator;
∇^2, $= \partial_{xx} + \partial_{yy}$, Laplace operator;
$\tilde{\nabla}^2$, $= [\alpha \partial_{\xi\xi} - 2/\beta \partial_{\xi\eta} + \gamma \partial_{\eta\eta} + J^2 (P \partial_\eta + Q \partial_\xi)]/J^2$, transformed Laplace operator.

Subscripts

0, reference point;
c, cylinder;
f, fusion;
i, interface;
R_c, based on R_c;
s, solid;
w, wall;
n, x, y, t, derivatives with respect to n, x, y, t;
ξ, η, τ, derivatives with respect to ξ, η, τ.

* This contribution is dedicated to Prof. F. Bošnjaković on the occasion of his 80th birthday.

Superscripts

(k),	iteration level;
$-$,	mean value.

1. INTRODUCTION

HEAT TRANSPORT during solid–liquid (melting) and liquid–solid (solidification) phase change plays an important role in numerous naturally occurring and technical processes. In many technical areas, such as casting technology, thermal energy storage design and nuclear power accident analysis, knowledge of the governing hydro- and thermodynamic phenomena is of great importance.

In the past, most of the analyses dealing with phase change problems have taken into account heat conduction as the sole heat transfer mechanism. Physical situations, however, in which heat conduction acts alone during phase change will not often be observed, because even small temperature variations in the melt can activate natural convection flow due to buoyancy forces. This effect, in turn violates the existing temperature distribution and can amplify the strength of the fluid flow in connection with a total change in the heat transfer characteristics. This interaction between two of the basic heat transport mechanisms is quite evident, when melting processes in latent heat-of-fusion thermal energy storage systems are investigated. Such systems offer advantages in some applications, i.e. solar energy systems, because of their great latent heat storage capacity, their small density variations during phase change and relatively small temperature differences in the operation phase. Pipes, or bundles of pipes, embedded horizontally in a phase change material (PCM) are possible technical system configurations which have been studied recently in a number of experimental and theoretical works [1–6].

Experimental investigations of melting process around a heated single tube or cylinder show clearly that only in the earliest stage of the process the heat transport mechanism is due to conduction alone, whereas natural convection becomes dominant subsequently. Photographs and shadowgraphs of the melting zone [1–6] demonstrate this fact. It can be observed that the melting front moves faster upward than downward in the course of the melting process and forms a liquid–solid interface, which is somewhat pear-shaped. Experiments by Goldstein and Ramsey [4] indicate that different shapes of the melting interface resulted in spite of similar initial and boundary conditions.

These experimental findings indicate, that the physical system is very sensitive to small disturbances during the test runs and to the provided initial and boundary conditions. Also an initial subcooling of the solid, which causes heat conduction in the frozen material, can markedly affect the melting characteristics of the system [7]. Therefore a legitimate attempt at an analytical solution with idealized physical conditions may be made in order to gain some insight into the underlying basic heat transfer mechanism of the melting process around a horizontal circular cylinder.

Closed form analytical solutions of the problem seem to be impossible due to the complexity of the governing equations and the additional difficulties associated with the moving interface. Until now only two papers were available [1, 8] which attacked this problem on the basis of perturbation methods. But the valid range of these series solutions is limited to situations, where natural convection flows are weak or the melting time is rather short. For longer melting times and fully developed convection flows a direct solution approach via discrete numerical methods seems to be reasonable.

Finite-difference solutions to the melting problem around a vertical tube were first presented by Sparrow *et al.* [9] who simplified the set of governing equations because of computational difficulties arising with the treatment of the interface. The finite element method was chosen by Gartling [10] to solve blockage problems in pipes and to investigate melting processes in materials with internal heat sources. In the present study a numerically generated body-fitted coordinate system was used, in conjunction with the finite difference approximation, to eliminate the complicating influence of an arbitrarily shaped physical region. This technique has also the capacity to handle timewise changing solution domains and is applied to natural convection problems with moving boundaries and phase change for the first time.

The physical model analyzed here is pictured schematically in Fig. 1. A horizontal cylinder of radius R_0 is embedded in the frozen phase change material, which is kept at fusion temperature. The melting process begins at the time $\tau = 0$, when the temperature of the cylinder is raised to a constant value above the fusion temperature. Heat conduction in the solid is

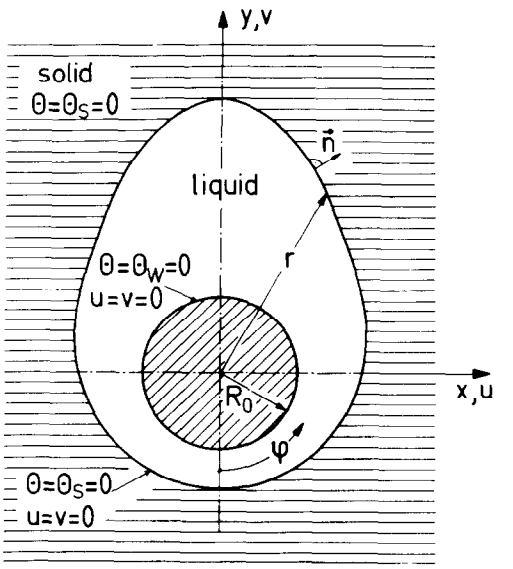

FIG. 1. Physical model.

neglected and symmetry to the vertical midplane (y-axis) is assumed in order to reduce the computational effort.

2. MATHEMATICAL FORMULATION

Under the assumption of an incompressible Newtonian fluid with constant properties (except the density), the governing equations, describing the conservation of mass, momentum and energy, may be written in Cartesian coordinates as follows:

$$\nabla \cdot \mathbf{w} = 0, \tag{1}$$

$$\mathbf{w}_t + (\mathbf{w} \cdot \nabla)\mathbf{w} = -\frac{1}{\rho_0}\nabla p + \nu\nabla^2\mathbf{w} + \mathbf{G}\left(\frac{\rho}{\rho_0} - 1\right), \tag{2}$$

$$T_t + \nabla \cdot (\mathbf{w}T) = a\nabla^2 T. \tag{3}$$

In studies of natural convection phenomena it is convenient to introduce a linear relationship between density and temperature into the buoyancy term, known as the Boussinesq approximation

$$\rho = \rho_0[1 - \bar{\beta}(T - T_0)]. \tag{4}$$

In the case of a 2-dim. flow of incompressible fluid the governing set of equations can easily be reduced by defining the stream function and vorticity as new dependent variables:

$$\mathbf{w} = \nabla \times \Psi, \tag{5}$$

$$\Omega = \nabla \times \mathbf{w}. \tag{6}$$

Substituting (5) into (6) and making use of (1) gives

$$\omega = -\nabla^2\psi, \tag{7}$$

while the elimination of pressure in (2) with the aid of (6) leads under consideration of (4) to the transport equation of vorticity:

$$\omega_t + \nabla \cdot (\omega\mathbf{w}) = \nu\nabla^2\omega + g\bar{\beta}\,T_x. \tag{8}$$

Equations (3), (7) and (8) should be brought into non-dimensional form by defining the following dimensionless variables and groups, in order to reduce the number of parameters:

$$\begin{aligned} (x, y)^* &= (x, y)/R_0, \\ (u, v)^* &= (u, v)R_0/a, \\ \theta &= (T - T_f)/(T_w - T_f), \\ \tau &= (at/R_0^2)(c_p(T_w - T_f)/h_f) = (Fo)(Ste), \\ Pr &= \nu/a, \\ Ra &= \bar{\beta}g\,R_0^3(T_w - T_f)/(a\nu). \end{aligned} \tag{9}$$

Asterisks denote dimensionless quantities, which have been omitted in the non-dimensional form of the governing equations given below:

$$Ste\,\omega_\tau + \nabla \cdot (\omega\mathbf{w}) = Pr\,\nabla^2\omega + Ra\,Pr\,\theta_x, \tag{10}$$

$$\omega = -\nabla^2\psi \tag{11}$$

$$Ste\,\theta_\tau + \nabla \cdot (\theta\mathbf{w}) = \nabla^2\theta. \tag{12}$$

To simplify the physical model under consideration, any variation of density through phase change as well as heat conduction in the solid is neglected. By assuming, that the solid is kept at its fusion temperature (Fig. 1), the entire heat transferred to the interface is utilized for melting and therefore determines the propagation speed and the shape of the moving interface.

This fact is stated by an energy balance at the melting front, which is written as:

$$-\lambda T_n = \rho h_f n_t. \tag{13}$$

In terms of dimensionless variables, equation (13) becomes

$$-\theta_n = n_\tau. \tag{14}$$

To complete the mathematical description of the problem the following initial and boundary conditions are specified:

$$\tau = 0: \quad \theta_w = \theta_f = 0 \tag{15a}$$

$$\tau > 0: \quad \theta_w = 1;\ u = v = 0 \quad \text{at the wall} \tag{15b}$$

$$\theta_s = \quad \theta_f = 0;\ u = v = 0 \quad \text{at the interface} \tag{15c}$$

$$\theta_n = 0;\ u = 0 \quad \text{at the symmetric line (vertical midplane)} \tag{15d}$$

The kinematic no-slip boundary conditions at the wall as well as at the solid–liquid interface are required on the assumption of constant density during phase change. The fact, that the physical region increases and changes its shape with time poses a moving boundary problem, in which the location of the interface is not known *a priori*, but is part of the overall solution. For the treatment of such problems in the context of discrete numerical methods there are basically two approaches which differ in the type of mesh used in the computation.

The fixed mesh approach employs a grid that is fixed in space and time and in which the phase boundary traverses the mesh system during the evolution process. One advantage of such an approach seems to be the ability to handle relatively complex interaction problems in conjunction with a simple formulation of the governing set of equations. However, a weak point of the fixed mesh approach is the treatment of all the boundary conditions at the moving interface, which is spread into a transition zone. This feature is important so far as the quality of any numerical solution with discrete methods is essentially dependent upon the approximation of the boundaries in a general solution domain and on the formulation of the required boundary conditions thereof. In fluid mechanical problems, strong gradients of the dependent variables appear at the boundaries, which favour, with the above-mentioned aspects in mind, the application of time dependent mesh systems. This alternative method for moving boundary calculations allows the computational grid to change with time, and maintaining the interface coincident with a particular

mesh line. So the implementation of latent heat effects and the formulation of boundary conditions is easy and straightforward. To handle arbitrarily shaped solution domains, a numerical mapping technique was chosen which generates a body-fitted coordinate system, and offers some possibilities in the spacing and structure of the grid system. By a transformation of the moving physical grid system, which is in general non-orthogonal, onto a rectangular and uniformly spaced computational domain, which is fixed in time and space, distortions of the physical grid system can easily be controlled and interpolations during the computational process can be minimized. The application of the mapping technique to the melting problem is described in the following section.

3. NUMERICAL PROCEDURE

3.1. *Transformation technique*

The employed numerical mapping technique (Fig. 2) is based on a method of automatic numerical generation of a general curvilinear coordinate system and was first developed and applied to fluid mechanical problems by Thompson *et al.* [11].

The boundary-fitted physical coordinate system is created by numerically solving the following system of elliptic equations:

$$\tilde{\nabla}^2 x = 0, \tag{16a}$$

$$\tilde{\nabla}^2 y = 0, \tag{16b}$$

with Dirichlet conditions at the boundaries. The transformed Laplace operator (definition see nomenclature) involves coordinate control functions P and Q, which may be chosen to influence the structure of the grid as desired. Under the assumption of symmetrical boundary conditions the solution domain is a simply connected region. For such a configuration it is possible to use an improvement proposed by Middlecoff and Thomas [12], which eliminates the problem of choosing relevant control functions. This method uses general source terms P and Q:

$$P(\xi, \eta) = \phi(\xi, \eta)(\xi_x^2 + \xi_y^2), \tag{17a}$$

$$Q(\xi, \eta) = \chi(\xi, \eta)(\eta_x^2 + \eta_y^2), \tag{17b}$$

where the parameters ϕ, χ are evaluated locally at the boundaries of the computational domain. The parameters at the interior grid points are then obtained by simple linear interpolation. Substitution of (17a, b) into (16a, b) and requiring that the given boundary values satisfy appropriate limiting forms of the resulting equations along the boundary of the computational domain, leads to the following equations for the evaluation of ϕ, χ:

$$\xi = \text{const}: \quad x_{\eta\eta} + \chi x_\eta = 0, \tag{18a}$$

$$y_{\eta\eta} + \chi y_\eta = 0, \tag{18b}$$

$$\eta = \text{const}: \quad x_{\xi\xi} + \phi x_\xi = 0, \tag{18c}$$

$$y_{\xi\xi} + \phi y_\xi = 0. \tag{18d}$$

Since there are always two equations to calculate one parameter, in principle either can be used. In practice, the best results are obtained by employing that equation for which the first derivative is maximal at a given point. With such a treatment all grid systems are well structured.

3.2. *Transformed governing equations*

To solve the given set of governing equations (10)–(12) with the corresponding boundary conditions on the computational rectangular field, all equations have to be transformed. This leads to the following, somewhat more complicated, equations and boundary conditions:

$$Ste\frac{\mathscr{D}\omega}{\mathscr{D}\tau} + L^\psi\omega = Pr\,\tilde{\nabla}^2\omega + Ra\,Pr\,L^y\theta, \tag{19}$$

$$\tilde{\nabla}^2\psi = -\omega, \tag{20}$$

$$Ste\frac{\mathscr{D}\theta}{\mathscr{D}\tau} + L^\psi\theta = \tilde{\nabla}^2\theta, \tag{21}$$

where the operators L^f F and $\Sigma\tilde{\nabla}^2$ are given in the nomenclature and $\mathscr{D}f/\mathscr{D}\tau$ is defined as

$$\frac{\mathscr{D}f}{\mathscr{D}\tau} = f_\tau - x_\tau L^x f + y_\tau L^x f. \tag{22}$$

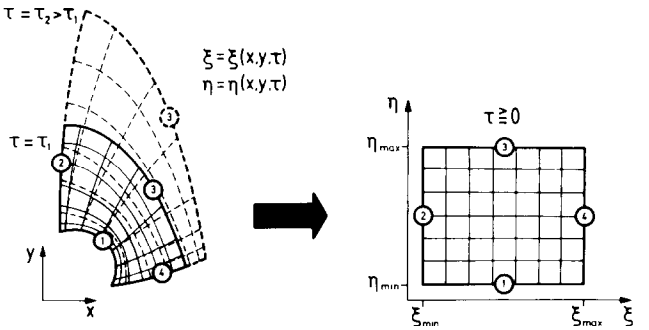

FIG. 2. Illustration of the transformation method.

Boundary conditions:

$$\xi = \xi_{\min}: \ \psi = 0; \ \omega = 0; \ \alpha\theta_\xi - \beta\theta_\eta = 0, \quad (23a)$$

$$\xi = \xi_{\max}: \ \psi = 0; \ \omega = 0; \ \alpha\theta_\xi - \beta\theta_\eta = 0, \quad (23b)$$

$$\eta = \eta_{\min}: \ \psi = 0; \ \omega = -\frac{\gamma\psi_{\eta\eta}}{J^2}; \ \theta = 1, \quad (23c)$$

$$\eta = \eta_{\max}: \ \psi = 0; \ \omega = -\frac{\gamma\psi_{\eta\eta}}{J^2}; \ \theta = 0, \quad (23d)$$

(23a, b) are symmetrical boundary conditions at the vertical midplane. The conditions, which move the boundary at $\eta = \eta_{\max}$(14), lead under consideration of (23d) to the following expression for the timewise change of the boundary grid points in the physical plane:

$$x_\tau = \frac{y_\xi}{J}\theta_\eta, \quad (24a)$$

$$y_\tau = -\frac{x_\xi}{J}\theta_\eta. \quad (24b)$$

3.3. *Re-zoning procedure*

If the conditions (24a, b) are applied rigorously in the context of the numerical mapping technique the grid can be deformed wildly under some circumstances, because all grid points move towards one point if the solid–liquid interface is concave, and spread to the lower and upper side if it is convex. To overcome this problem an implicit re-zoning process is used to hold the desired structure of the grid system.

This process is accomplished by spline interpolation of the boundary grid points along the solid–liquid interface at time levels τ and $\tau + \Delta\tau$ to redistribute the grid points at the time level $\tau + \Delta\tau$ without loss of accuracy. Since the numerical generation of the physical coordinate system consists of the solution of a Dirichlet problem, well distributed boundary points lead automatically to a properly structured physical net. Coordinate systems created with this method are shown for three different times in Fig. 3.

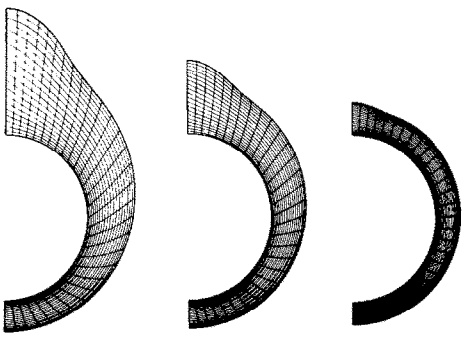

FIG. 3. Grid systems at different times.

3.4. *Computational details*

The transformed plane, which is a rectangular domain, is covered by a uniform mesh whose coordinates are denoted by the integer variables i and j, where

$$(\xi, \eta) = (\xi, \eta)_{\min} + (i, j) - 1 \quad 1 \le i, j \le IMAX, JMAX \quad (25)$$

Using this convention, variables at grid points are denoted by $f(i, j)$. Now it is convenient to define the following set of finite difference operators:

$$\delta_\xi f = f(i+1, j) - f(i, j), \quad (26a)$$

$$\bar{\delta}_\xi f = f(i, j) - f(i-1, j), \quad (26b)$$

$$2A_\xi f = f(i+1, j) + f(i, j), \quad (26c)$$

$$2\bar{A}_\xi f = f(i, j) + f(i-1, j). \quad (26d)$$

With these definitions the central difference approximations of the first, second and mixed derivative may be written as:

$$f_\xi \simeq \bar{A}_\xi(\delta_\xi f), \quad (28)$$

$$f_{\xi\xi} \simeq \delta_\xi\delta_\xi f, \quad (29)$$

$$f_{\xi\eta} \simeq \bar{A}_\xi\{\delta_\xi[\,|\,\bar{A}_\eta(\delta_\eta f)]\}. \quad (30)$$

For the derivatives with respect to η similar expressions can be obtained. With the exception of the convection terms, all terms of the governing equations (19)–(21) are expressed by the approximations (28)–(30). There are basically two alternative ways to approximate the convection terms in (19) and (21), first to use the central difference approximations (CDA) and second to use one-sided finite difference expressions (UDA) or combinations thereof. Although the first method has a second order truncation error it leads to numerical instability for Reynolds numbers greater than 2 based on the mesh width. The reason for this is, that the coefficient matrix of the finite difference analogue does not remain diagonal dominant. On the other hand, by employing forward or backward difference approximations, the instability can be circumvented, but some numerical diffusion will be introduced [13]. Since the produced artificial viscosity increases with increasing Rayleigh numbers, the results will deviate more and more from those of the 2nd-order central difference expressions. Two possible schemes for the approximation of the convection terms are:

$$\text{CDA:} \quad (fF)_\xi \simeq \bar{A}_\xi[\delta_\xi(fF)], \quad (31)$$

$$\text{UDA:} \quad (fF)_\xi \simeq (S^- f)(\delta_\xi F) + (S^+ f)(\delta_\xi F), \quad (32)$$

where the shifting operator S is defined as

$$S^\pm f = 0.5\,(f \pm |f|). \quad (33)$$

The algebraic set of equations is solved simultaneously by the Strongly Implicit Procedure (SIP) [14]. This solution technique has been successfully applied to free convection and conduction problems by the present authors [15, 16], where further details of the method are given. Therefore only the main aspect, which favours the application of SIP is described here.

By using matrix notation, SIP leads, starting with the original system of equations

$$\mathbf{MX} = \mathbf{Z} \tag{34}$$

to the following iteration procedure:

$$\mathbf{M} = \mathbf{LU}, \tag{35a}$$

$$\mathbf{L}^{(k)}\mathbf{V}^{(k+1)} = \mathbf{R}^{(k)}, \tag{35b}$$

$$\mathbf{U}^{(k)}\Delta\mathbf{X}^{(k+1)} = \mathbf{V}^{(k+1)}. \tag{35c}$$

In the aforementioned equations $\mathbf{M}$ is the altered coefficient matrix, so that a sparse $\mathbf{LU}$ decomposition is possible, $\mathbf{R}$ is the residual vector, and $\Delta\mathbf{X}^{(k+1)}$ is defined as $\mathbf{X}^{(k+1)} - \mathbf{X}^{(k)}$, where $\mathbf{X}$ is the solution vector.

Now SIP offers the possibility to get numerical stability by using the approximation of (32) for the coefficient matrix $\mathbf{M}$ and still permits to obtain central difference accuracy by the application of (31) for the residual vector $\mathbf{R}$. Since it is impossible to start the computations with an infinitly small volume, the initial temperature distribution and the appropriate time must be calculated for an assumed thin and concentric melt region. In view of the fact that at the beginning of the melting process heat conduction dominates, analytical but only one-dimensional solutions exist and are given by Eckert and Drake [17]. For the small Stefan numbers in conjunction with the very thin initial melt layer thickness an approximate solution yields sufficiently accurate results for the starting time and temperature distribution. The solution of the finite difference analogue of (16, 19, 20, 21) is performed in such a manner that (19), (20) and (16), (21) are solved in a coupled and simultaneous way, because these equations have the strongest coupling.

The computations were started with a time interval $\Delta\tau = 10^{-4}$, which was raised, depending on the parameters, during the iteration process up to values of 10^{-3}. The next time step was started, when the following criterion

$$\left|\frac{f^{(k+1)}(i,j) - f^{(k)}(i,j)}{\operatorname{Max} f^{(k+1)}(i,j)}\right| < 5 \cdot 10^{-5} \tag{36}$$

was satisfied for all variables.

The desire to use small mesh intervals for higher accuracy had to be compromised by limitations imposed by the available computing equipment (DEC-PDP 10/70). So, all computations were performed with a grid system containing 31 × 21 nodal points as a compromise between accuracy and computing time.

4. RESULTS AND DISCUSSION

All computations presented have been performed with a constant Prandtl number and under the assumption of a constant tube diameter. This has been done because the numerical results by Sparrow *et al.* [9] have not indicated any significant dependence on Prandtl number in the range $7 \leqq Pr \leqq 50$. The dependence on the Stefan number is solely taken into account by the dimensionless time τ, which is a product of Fo and Ste. In the range $0.05 \leqq Ste \leqq 0.15$ no additional parametric dependence on Ste was found [9]. This has been verified for the present configuration in some test runs. In order to give an idea about the shape of the melting zone during the evolution process, interface contours are discussed first, followed by some representative temperature and flow field distributions. Finally the calculated heat transfer results are presented.

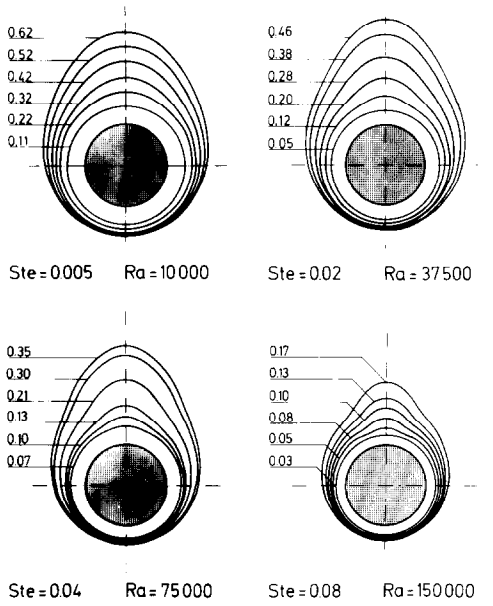

FIG. 4. Time history of the melted region for various Rayleigh and Stefan numbers (dimensionless time τ as parameter).

Figure 4 shows transient interface positions for various Rayleigh and Stefan numbers. From the calculated shapes, only at the very beginning a dominating role of heat conduction can be deduced. However, after this short period the melting front moves concentrically outward, an increasing natural convection flow alters this kind of a nearly uniform propagation. The formation of a thermal plume above the cylinder gradually influences the local heat transfer rate and therefore the melting characteristics of the system. At the top of the melt region the impinging plume strongly affects the melting process and leads to a faster upwardly directed growth of the interface. An inverse effect can be stated in the lower part of the annulus. The relatively cold fluid flowing down along the solid–liquid interface inhibits heat transport due to conduction in this part. At the bottom these counteracting transport mechanisms lead to an almost total stop of the melting process. It is evident, that the limiting gap width at the bottom becomes smaller with

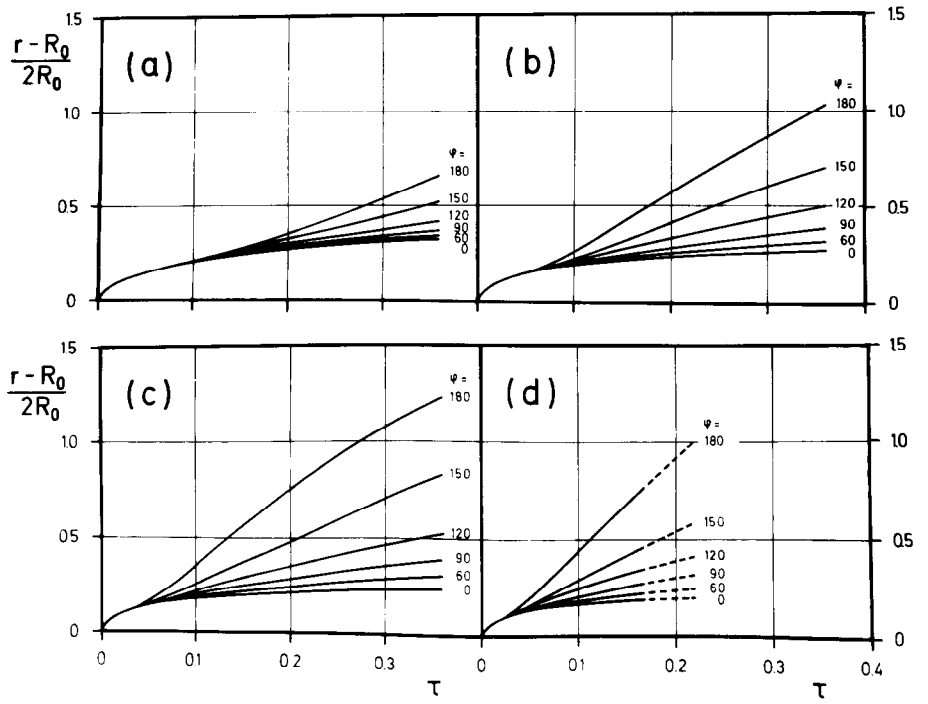

FIG. 5. Local interface positions as function of time (a) Ra = 10,000, Ste = 0.005; (b) Ra = 37,500, Ste = 0.02; (c) Ra = 75,000, Ste = 0.04; (d) Ra = 150,000, Ste = 0.08.

increasing Rayleigh number. Inspection of the time-wise development of the melt zone for various temperature differences (expressed by a proportional change of Ra and Ste), reveals a general trend: the gradients of the interface slope in the top region of the melting zone increase with increasing Ra and Ste. In this context the case for Ra = 150,000 is noteworthy. Turning points in the interface contours indicate the formation of 'keyhole' shapes, which were also observed in the experiments by Goldstein and Ramsey [4].

For a quantiative description of the melting front propagation a suitable and more instructive representation is chosen. In Fig. 5 the ratio of the radial melt layer thickness to the tube diameter is plotted as a function of the dimensionless time τ. The curves are parameterized by the angle of perimeter. In all graphs the concentric movement of the phase boundary due to heat conduction as well as the temporal validity of that transport mechanism can be recognized. After natural convection sets in a faster propagation of the interface in the upper portion of the melt zone causes a fanning out of the corresponding curves, with increasing gradients for advancing angles of perimeter. Higher Rayleigh numbers cause a faster growth of the melt layer thickness in the top region. After a short transition period the curves reveal a nearly linear time

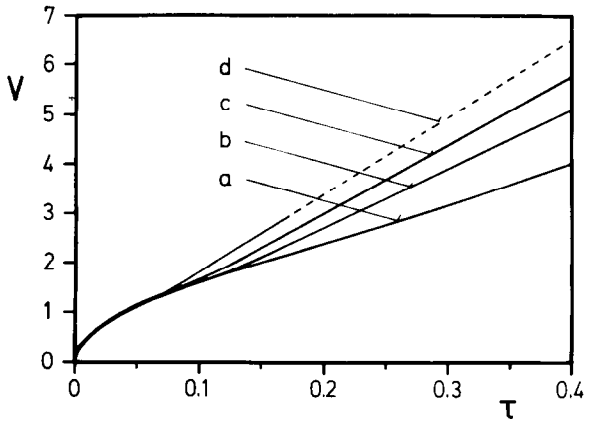

FIG. 6. Melted volume as function of time (a) Ra = 10,000, Ste = 0.005; (b) Ra = 37,500, Ste = 0.02; (c) Ra = 75,000, Ste = 0.04; (d) Ra = 150,000, Ste = 0.08.

dependence, for constant angle condition. The increase of molten volume with time reveals an analogous behaviour (Fig. 6). For the regime of developed natural convection, an approximately linear variation of the molten volume results. This was confirmed by Goldstein and Ramsey [4] as well as by Bathelt *et al.* [3], investigating experimental melting around a heated horizontal cylinder for a constant heat flux condition. After a short period of melting the recorded temperature distributions around the cylinder surface [4] proved to be quite uniform, so that the boundary conditions seem to be comparable. The nature of the resulting flow pattern (streamlines and temperature fields) in the course of the melting process is well illustrated by Fig. 7 for six different times. As a representative example the case for $Ra = 37{,}500$ and $Ste = 0.02$ is presented.

The first picture ($\tau = 0.054$) characterized by concentric isotherms and a weak and symmetric flow field, is valid for the very first moments where heat conduction dominates. The maximum value of streamfunction is located at the horizontal midplane of the annulus. Time level $\tau = 0.124$ can be related to a transition phase, where heat transfer by conduction is superseded by convection in the upper portion of the melt zone. With increasing time, a thermal plume develops by which hot liquid is conveyed to the top of the gap. Thus heat transfer at the upper stagnation point is improved and leads to a faster propagation of the melting front. The expansion of the melt zone in the upper part is accompanied by a shifting of the vortex center to a position of about 18° from the top ($\tau = 0.457$). At the time $\tau = 0.457$, the temperature distribution shows a nearly isothermal core in the vicinity of the centre of rotation and strong gradients around the cylinder and along the upper part of the interface. This behaviour indicates the existence of a flow regime in which heat transfer is governed mainly by boundary layers. The temperature fields in the lower part of the melt zone reveals, that the heat transfer to the phase boundary and its movement respectively, decrease monotonically.

Attention is now focused upon the heat transfer results. In Fig. 8(a) the instantaneous local heat transfer coefficients at the cylinder surface as well as at the interface are plotted vs the dimensionless time τ. High values of local coefficients at the very beginning associated with a sharp decrease are characteristic for transient heat conduction. The end of this period of nearly 1-dim. behaviour is indicated by a spanwise spreading into individual curves. The local heat transfer coefficients at the cylinder surface pass a minimum, which is attained for greater angles at later times and rise smoothly in the following time history. At the interface the situation is somewhat different. For parameter values $\varphi < 120°$ a monotonic decrease is observed, in contrast to the upper part of the interface, where after a minimum, a maximum of the corresponding curves can be recognized. This is pronounced especially for values $\varphi \to 180°$. With increasing time the local heat flux at all positions decreases almost linearly. This timewise variation of the local heat transfer coefficients after transition was also observed experimentally by Goldstein and Ramsey [4]. From Fig. 8(b) it can be stated that the transition stage during the melting process is shorter for higher Rayleigh numbers. In order to find some characteristic trends only the limiting parameters $\varphi = 0°$ and $\varphi = 180°$ are displayed for various Rayleigh numbers. A comparison with Fig. 8(a) shows qualitatively the same behaviour in the whole range of studies. The faster onset of natural convection as well as the increasing strength of fluid motion for higher Rayleigh

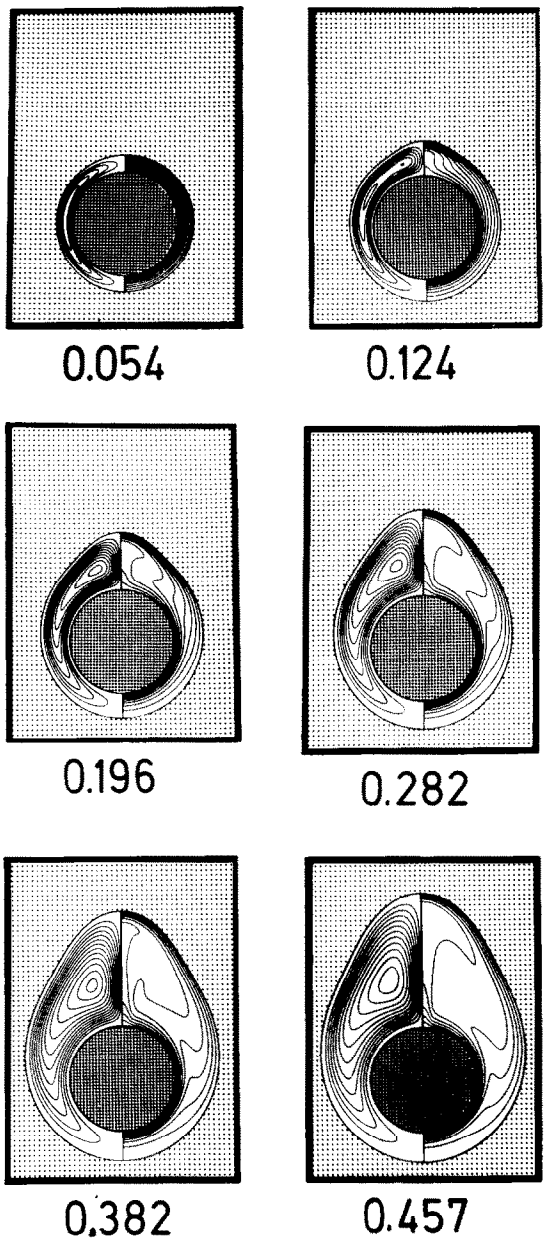

FIG. 7. Flow pattern and temperature distributions at different times τ for $Ra = 37{,}500$ and $Ste = 0.02$.

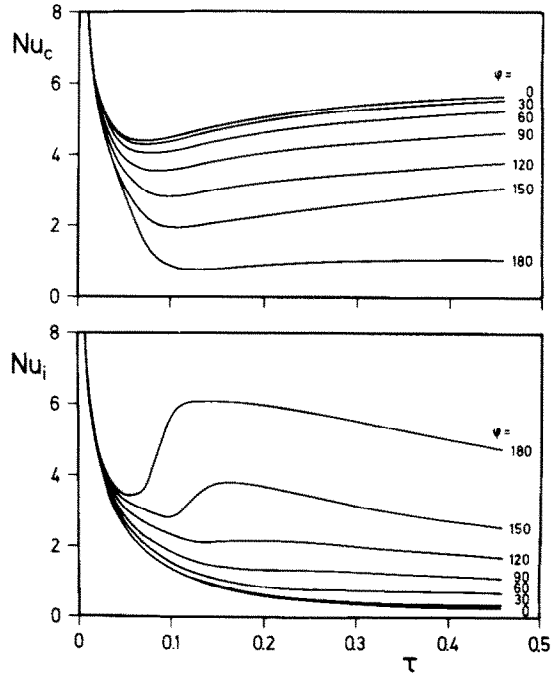

(a)

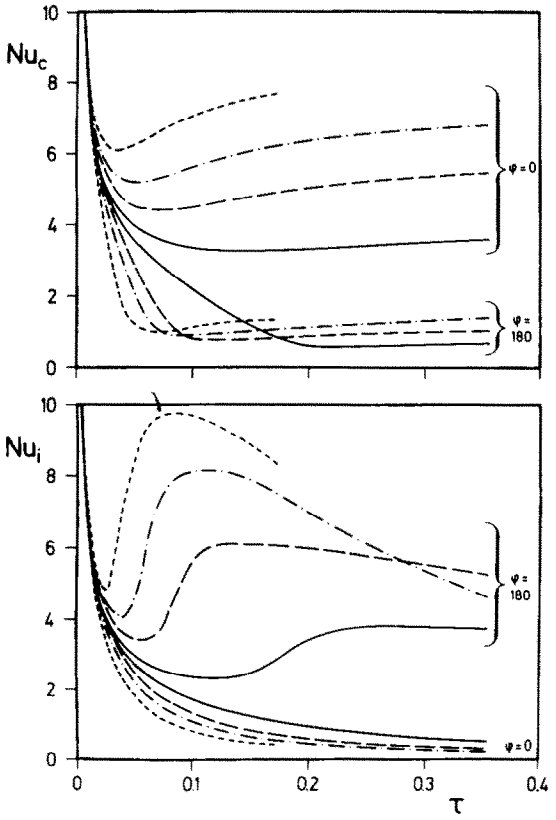

(b)

FIG. 8. Local heat transfer coefficients as function of time (a) $Ra = 37{,}500$, $Ste = 0.02$; (b) —— $Ra = 10{,}000$, $Ste = 0.005$; – – $Ra = 37{,}500$, $Ste = 0.02$; – · – · $Ra = 75{,}000$, $Ste = 0.04$; – – – $Ra = 150{,}000$, $Ste = 0.08$.

numbers tends to accentuate the above-mentioned effects.

In order to find a general correlation for the experimentally determined overall heat transfer coefficients Bathelt and Viskanta [5] proposed an empirical correlation in the form of $\overline{Nu_{R_c}} = C \cdot (Ra_{R_c}/Ste)^n$. The characteristic length R_c of the melt layer thickness is defined as:

$$R_c = \left(\frac{R_0}{\pi}\int_0^{\pi} r\,d\varphi\right)^{1/2} \cdot \ln\left(\frac{1}{\pi R_0}\int_0^{\pi} r\,d\varphi\right). \quad (37)$$

An appropriate representation of the calculated and the experimental results is given in Fig. 9. It is quite evident that the experimental results [5] can be well approximated by the correlation proposed. The calculation, in contrast, shows a different behaviour. For the disagreement between the experimental and numerical data there can be many reasons. As pointed out by [18], some errors could have been introduced in the determination of the melting rate from photographs, by numerical differentiation of the interface positions. An essential influence could also be expected from the occurrence of an oscillating plume, in the range of Rayleigh numbers studied experimentally.

From a physical point of view the numerical results seem to be more reasonable. After a transition period which is governed by heat conduction, increasing Rayleigh numbers should lead to greater values of the overall heat transfer coefficient for the same melt layer thickness as expressed by the calculated results. This is a consequence of the fact that in the quotient Ra_{R_c}/Ste the driving temperature difference is eliminated and therefore this term only provides geometrical information. Moreover the use of R_c as a characteristic length seems not to be a good choice, since for the practical application an additional relation between the geometrical form and time must be provided. Therefore a representation of the overall heat transfer coefficients, based on the constant cylinder radius, as function of time should be favoured. The calculated overall heat transfer coefficients at the cylinder surface as well as at the interface are plotted in Fig. 10 in form of $\overline{Nu}/Ra^n$ vs time τ. The graphs show, that after a transition stage, all curves coincide with the nearly constant value of quasi-steady melting. Since this phase is independent of time the quasi-steady melting process around a circular cylinder can well be approximated by

$$\overline{Nu} = C \cdot Ra^n, \quad (38)$$

where $C \cong 0.13$, $n = 1/3$ for the cylinder and $C \cong 0.14$, $n = 1/4$ for the interface give only small deviations.

5. CONCLUDING REMARKS

The characteristics of the melting process around a circular cylinder were analyzed. A timewise changing grid system in conjunction with the finite difference method was used to handle the expanding physical domain. The boundary-fitted coordinate method has

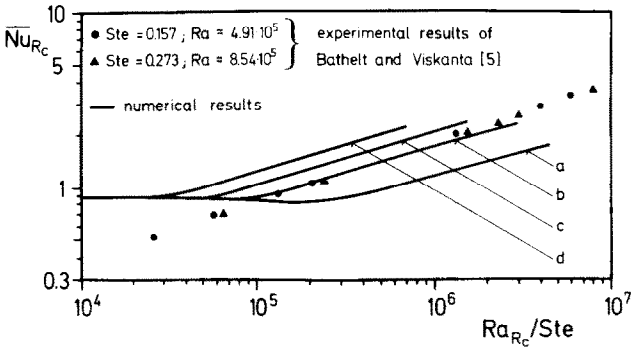

FIG. 9. Overall heat transfer coefficients at the solid–liquid interface as function of Ra_{R_c}/Ste (a) Ra = 10,000, Ste = 0.005; (b) Ra = 37,500, Ste = 0.02; (c) Ra = 75,000, Ste = 0.04; (d) Ra = 150,000, Ste = 0.08.

proved to be a flexible tool for the treatment of moving boundary problems. The shape of the molten region as well as the flow and temperature distributions were numerically obtained by finite difference approximations of the governing equations. The results of the present study can be summarized as follows:

As expected from available experimental data, natural convection is the dominating mode in the heat transfer mechanism for almost the whole melting process. In any analysis of such processes the effect of the fluid motion may not be neglected. At the very beginning of the process heat conduction acts solely but will soon be superseded by natural convection. The onset of the convective flow initiates the transition period whose duration is affected by the Rayleigh number. Experimental methods can hardly analyze this phase. During transition the local heat transfer coefficients for particular values of Ra and φ pass extrema. In the range of the Rayleigh numbers studied, the quasi-steady state of the melting process can be correlated by $\overline{Nu} = C \cdot Ra^n$.

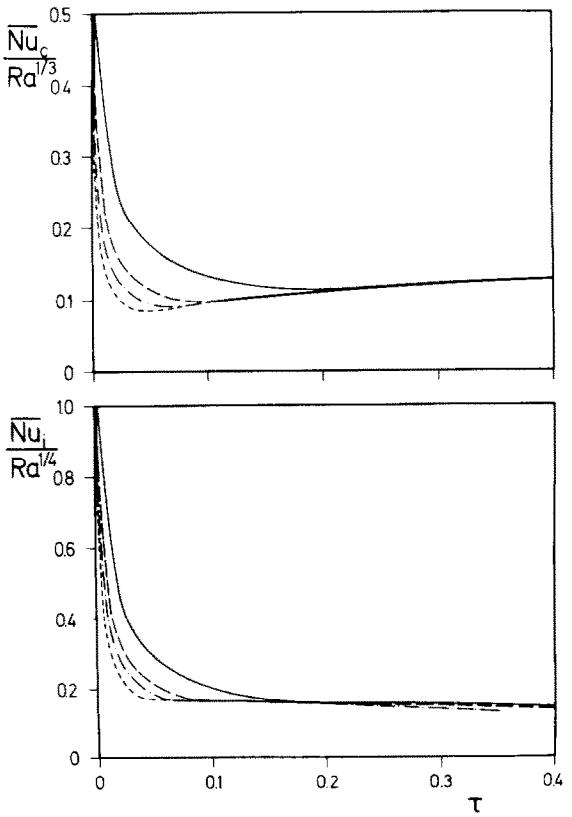

FIG. 10. Overall heat transfer coefficients at the cylinder and at the liquid–solid interface. —— Ra = 10,000, Ste = 0.005; – – Ra = 37,500, Ste = 0.02; – · – · Ra = 75,000, Ste = 0.04; – – – Ra = 150,000, Ste = 0.08.

REFERENCES

1. R. D. White, A. G. Bathelt, W. Leidenfrost and R. Viskanta, Study of heat transfer and melting from a cylinder imbedded in a phase change material, ASME Paper No. 77-HT-42 (1977).
2. E. M. Sparrow, R. R. Schmidt and J. W. Ramsey, Experiments on the role of natural convection in the melting of solids, *J. Heat Transfer* **100**, 11–16 (1978).
3. A. G. Bathelt, R. Viskanta and W. Leidenfrost, An experimental investigation of natural convection in the melted region around a heated horizontal cylinder, *J. Fluid Mech.* **90**, 227–239 (1979).
4. R. J. Goldstein and J. W. Ramsey, Heat transfer to a melting solid with application to thermal energy storage systems, in *Heat Transfer Studies: Festschrift for E. R. G. Eckert*, pp. 199–206. Hemisphere, New York (1979).
5. A. G. Bathelt and R. Viskanta, Heat transfer at the solid-liquid interface during melting from a horizontal cylinder, *Int. J. Heat Mass Transfer* **23**, 1493–1503 (1980).
6. R. Viskanta, A. G. Bathelt and N. W. Hale, Jr., Latent heat-of-fusion energy storage: experiments on heat transfer during solid–liquid phase change, in *Proc. 3rd Miami Int. Conf. on Alternative Energy Sources*, 15–17 Dec. 1980, Bal Harbour, Florida.
7. E. M. Sparrow, S. Ramadhyani and S. V. Patankar, Effects of subcooling on cylindrical melting, *J. Heat Transfer* **100**, 395–402 (1978).
8. L. S. Yao and F. F. Chen, Effects of natural convection in the melted region around a heated horizontal cylinder, *J. Heat Transfer* **102**, 667–672 (1980).
9. E. M. Sparrow, S. V. Patankar and S. Ramadhyani, Analysis of melting in the presence of natural convection in the melt region, *J. Heat Transfer* **99**, 520–526 (1977).
10. D. K. Gartling, Finite element analysis of convective heat transfer problems with change of phase, in *Proc. First Int. Conf. on "Numerical Methods in Laminar and Turbulent Flow"*, 17–21 July 1978, Swansea.
11. J. F. Thompson, F. C. Thames and C. W. Mastin, Automatic numerical generation of body-fitted curvi-

linear coordinate system containing any number of arbitrary two-dimensional bodies, *J. computat. Phys.* **15**, 299–319 (1974).
12. J. F. Middlecoff and P. D. Thomas, Direct control of the grid point distribution in meshes generated by elliptic equations, in *Proc. 4th AIAA Computat. Fluid Dyn. Conf.* pp. 175–179, Williamsburg, VA. (1979).
13. P. J. Roache, *Computational Fluid Dynamics*. Hermosa, Albuquerque, NM. (1976).
14. S. Nakamura, *Computational Methods in Engineering and Science*, pp. 123. Wiley, New York (1977).
15. U. Projahn, H. Rieger and H. Beer, Heat conduction in anisotropic composites of arbitrary shape, *Wärme- u. Stoffübertragung* **15** (1981).
16. U. Projahn, H. Rieger and H. Beer, A numerical analysis of laminar natural convection between concentric and eccentric cylinders, *Num. Heat Transfer* **4** (1981).
17. E. R. G. Eckert and R. M. Drake, *Analysis of Heat and Mass Transfer*, pp. 222. McGraw-Hill, New York (1972).
18. R. Viskanta, private communication.

ANALYSE DES MECANISMES DE TRANSFERT THERMIQUE PENDANT LA FUSION AUTOUR D'UN CYLINDRE CIRCULAIRE ET HORIZONTAL

Résumé—On étudie par des méthodes numériques la fusion autour d'un cylindre circulaire et horizontal noyé dans un matériau à changement de phase. La conduction et la convection thermique sont prises en compte pour traiter ce problème à frontière mobile. Des difficultés associées à la structure complexe du domaine de changement physique au cours du temps (région de fusion) ont été surmontées avec succès en appliquant une technique de maillage numérique (coordonnées adaptées à la géométrie).

Des solutions numériques ont été obtenues pour des nombres de Rayleigh allant jusqu'à $1{,}5 \cdot 10^5$, des nombres de Stefan entre 0,005 et 0,008 et pour $Pr = 50$. Les résultats sont discutés en détail et ils indiquent que l'influence de la convection naturelle a été considérée dans tous les cas.

Zusammenfassung—Der Schmerlzvorgang um einen, in eine schmelzfähige Substanz eingebetteten, waagrecht liegenden Zylinder wurde mit Hilfe einer numerischen Methode untersucht. Beide Wärmetransportmechanismen—Wärmeleitung und Konvektion- wurden bei der Behandlung dieses Problems mit sich bewegenden Grenzflächen berücksichtigt. Schwierigkeiten, bedingt durch die komplexe Form des sich zeitlich ändernden Lösungsgebiets (Schmelzraum), ließen sich durch die Anwendung einer numerischen Transformationsmethode beseitigen.

Die numerischen Berechnungen umfassen Lösungen für Rayleigh-Zahlen bis $Ra = 1.5 \cdot 10^5$, Stefan-Zahlen im Bereich $0.005 \leqq Ste \leqq 0.08$ und einer Prandtl-Zahr $Pr = 50$. Die Ergebnisse werden ausführlich diskutiert und zeigen, daß bei der analytischen Betrachtung derartiger Schmelzprozesse der Einfluß der natürlichen Konvektion unter keinen Umständen vernachlässigt werden darf.

ИССЛЕДОВАНИЕ МЕХАНИЗМА ПЕРЕНОСА ТЕПЛА ПРИ ПЛАВЛЕНИИ ВОКРУГ ГОРИЗОНТАЛЬНОГО КРУГЛОГО ЦИЛИНДРА

Аннотация — Численными методами анализируется процесс плавления вокруг нагреваемого горизонтального круглого цилиндра, помещенного в материал, претерпевающий фазовый переход. В рассматриваемой задаче с движущейся границей учитываются как теплопроводность, так и конвекция. Использование численного метода отображений (координаты, связанные с телом) позволило избежать трудностей, возникающих при рассмотрении сложной структуры изменяющейся во времени физической области (области плавления). Численные решения получены для чисел Релея до $Ra = 1{,}5 \cdot 10^5$, чисел Стефана в диапазоне $0{,}005 \leqq Ste \leqq 0{,}08$ и для $Pr = 50$. Подробно обсуждены результаты и показано, что во всех случаях следует учитывать влияние естественной конвекции.